

Three-dimensional chemical analysis of tungsten probes by energy dispersive x-ray nanotomography

Z. Saghi, X. Xu, Y. Peng, B. Inkson, and G. Möbus^{a)}

Department of Engineering Materials, University of Sheffield, Sheffield S1 3JD, United Kingdom

(Received 2 October 2007; accepted 29 November 2007; published online 18 December 2007)

The chemical distribution of oxide layers around functional tungsten nanotips is studied using electron tomography. Three-dimensional element distribution functions are derived for such tips, giving insight into the subsurface chemistry. Energy dispersive x-ray (EDX) spectroscopy is coupled to computed tomography to reconstruct slices across the tip. It is finally shown how the surface reconstruction by geometric tomography from annular dark field scanning transmission electron microscopy images can be combined with EDX tomography reconstructions to reduce backprojection artefacts and improve the sharpness of the surface contours. © 2007 American Institute of Physics. [DOI: 10.1063/1.2826273]

Tungsten tips have developed into the most widely used nanoprobe for applications ranging from scanning tunneling microscopy¹ (STM) to nanoindentation² and nanomanipulation in the scanning electron microscopes (SEM) and focused ion beam microscopes.³ In particular, they are suitable for nanoindentation and contacting experiments inside a transmission electron microscope (TEM).⁴ Three criteria will most crucially influence the performance of the tips in all of the mentioned applications: (i) the surface chemistry of the tip as fabricated, which will mostly be affected by a thin oxide film and sometimes by carbon-based contamination layers, (ii) the surface morphology and tip shape, which is mostly too complex in detail to just being described by a single figure of curvature radius, and (iii) the degradation of the tip in service (deformation, change of contact zone, further contamination, and material transfer). It has become common practice to estimate the performance of these criteria by two complementary strategies: firstly, in STM service, the tip shape and its possible degradation can be estimated by deconvolution from the images themselves, however, restricted to the immediate contact zone. Secondly, observation of the tip in the TEM will give a projection image of the entire tip with an adaptable field of view. In the present work, our aim is to demonstrate how chemically sensitive (or “spectroscopic”) electron tomography in the TEM can be employed to provide three-dimensional (3D) details on surface layers, while at the same time provide true 3D morphology by avoiding projection artefacts. This kind of nanoscale resolution tomography⁵ has been recently made applicable to crystalline objects by suppressing crystal lattice plane orientation contrast, which would destroy the projection relationship. Three incoherent modes seem to be most promising, including energy filtered TEM,⁶ annular dark field scanning TEM (ADF-STEM) Z contrast,⁷ and energy dispersive x-ray (EDX) mapping. In this work, we explore the latter mode, in particular.

Tungsten tips were prepared by electrochemical etching: 100 μm diameter tungsten wires were etched in an electrolyte of 2M NaOH with a graphite rod cathode. A tip maker of Nanomagetics Instruments Ltd., UK, provides automatic switch off. By the variation of etching currents, the tip

shapes and tip radii could be varied, with the maximum etching current being 7 mA and the typical time of etching being 15 min. We explore our tips by direct mounting on a high tilt tomography holder using a special cylindrical specimen mount. This specimen configuration helps to reach high tilt angles in an ultrasmall lens gap and to prevent x-ray detector shading.⁸ We used a JEM 2010F FEGTEM (Jeol, Japan) equipped with an ultrathin window EDX detector (Oxford Instruments, UK).

Figure 1(a) shows the ADF-STEM image of a W tip with gold nanoparticles attached to its surface for alignment purposes. For thick samples, such as the tip in Figs. 1(b) and 2, ADF-STEM imaging mode suffers from a nonmonotonic intensity-thickness relationship, which appears first as saturation and later as contrast inversion due to high angle scattering (one kind of “absorption” as electrons fail to reach the detector) at higher thicknesses [Fig. 2(a)]. Tomography reconstruction from such nonmonotonic projection images would contain unreliable quantitative information. On the other hand, EDX imaging mode tolerates larger thicknesses, as illustrated by an EDX W map with horizontal line profile

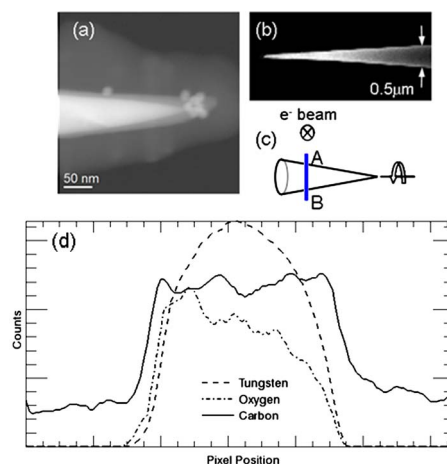


FIG. 1. (Color online) (a) ADF-STEM image of a 100 nm thick tungsten tip with gold particles attached to its surface. (b) ADF-STEM image of a 500 nm thick tungsten tip used for the EDX linescan tomography experiment showing the saturation and absorption artefacts at large thickness. (c) EDX linescan tomography acquisition setting. (d) W $L\alpha$, O-K, and C-K EDX signals along AB at 0° tilt angle.

^{a)}Electronic mail: g.moebus@sheffield.ac.uk.

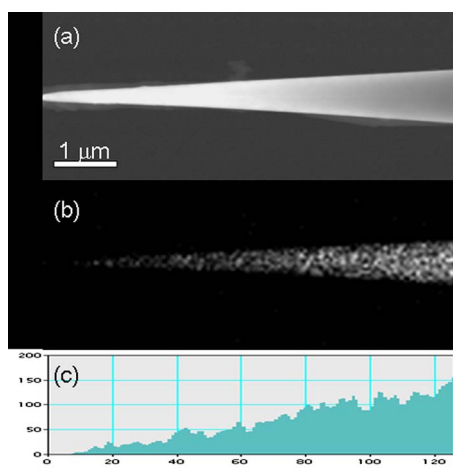


FIG. 2. (Color online) Image of a $1 \mu\text{m}$ thick tungsten tip. (a) ADF image affected by the saturation and absorption. [(b) and (c)] Tungsten mapping by EDX with a horizontal line profile along the axis of the tip.

in Figs. 2(b) and 2(c), and hence can be used for the 3D chemical analysis of specimens much thicker than 100 nm. The ADF-STEM tilt series of the tip in Fig. 1(a) was acquired from -65° to $+65^\circ$ with 5° increment. The EDX linescan tilt series of the tip in Fig. 1(b) was acquired by tilting the specimen holder from -70° to $+50^\circ$ with a tilt increment of 10° and by multiple fast scanning the beam across the line AB until the noise is sufficiently low at each tilt angle [see Fig. 1(c)]. Across the tilt series, the line AB was kept fixed and was defined by its distance to the apex of the tip. For an ideal tomographic reconstruction, a high tilt range as close as possible to 180° and a tilt increment as small as possible are required. The tilt increment chosen for the EDX linescan experiment was a compromise between two criteria, assuming that the total acquisition time $T = n \cdot t$ (n being the number of tilt angles and t the acquisition time per tilt angle) for the entire experiment as fixed: (i) the attempted reconstruction resolution is inversely proportional to the tilt increment and therefore suggests a split of T into $n \cdot t$ with large n and (ii) the signal-to-noise ratio and alignment precision of each image are proportional to the individual exposure time $t \sim T/n$, and thus inversely related to the number of increments. In our case, the total acquisition time T , and thus the angular range and tilt increment, was limited by the carbon contamination and possible sample bending, which become significant after several hours of highly focused electron beam exposure. Figure 1(d) shows the W L α , O-K and C-K EDX signals along the line AB at 0° tilt angle. The alignment and 3D reconstruction from the ADF-STEM tilt series were performed using IMOD software.⁹ A projected view from the reconstructed 3D data is shown in Fig. 3(a): the tungsten core appears in red and is covered by a tungsten oxide layer, highlighted in green. The carbon contamination is shown in blue. A slice through the volume [Fig. 3(b)] shows a well resolved sharp transition from the core to the shell. The volume can also be displayed as isosurface, and a threshold value can be adjusted to segment the core, as shown in Fig. 3(c), or the outer surface of the tip defined by the oxide as in Fig. 3(d).

The EDX linescan series was exported to interactive data language IDL (RSI, USA) and an in-house backprojection code was applied for the reconstruction. Figure 4 shows the distribution of (a) W, (b) oxygen, and (c) carbon in the cross

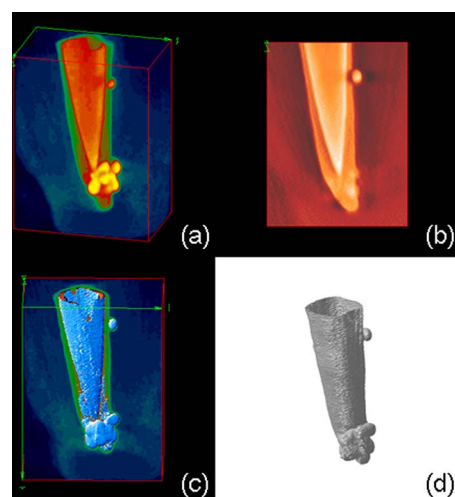


FIG. 3. (Color online) Tomographic reconstruction of tungsten tip morphology from ADF-STEM tilt series: (a) voxel projection, (b) slice through the volume, (c) isosurface of the core superimposed on the voxel projection, and (d) isosurface of the outer WO_3 layer and attached gold nanoparticles.

section along AB, and the line contours were added to emphasize compositional changes. The red-green-blue (RGB) map of Fig. 4(e) shows the superposition of W and O in the shell (from WO_3), and a C contamination layer. Two detailed observations need to be pointed out: (i) From Fig. 4(b), the oxygen distribution is not fully annular. This is suspected to be due to the varying W depth crossed by the x rays on the way to the detector.⁸ (ii) The C projection signal in Fig. 1(d) appears as a superposition of a flat and an annular signal, which is explained by the overlap of the carbon-specific peak with the background signal coming from the zero peak tail and the Bremsstrahlung continuum. Furthermore, residues of the “missing wedge” of nonacquired tilt angles⁵ appear in Figs. 3 and 4 as an elongation in the z direction and anisotropic resolution. We introduce here a new methodology for reducing the star artefacts induced by the large tilt increment. The ADF-STEM linescan tilt series acquired in parallel to the EDX maps along the same cross-section AB [Fig. 1(c)] can be used to extract the object contour, despite the strong high angle scattering/absorption effect. For illustration, the ADF-STEM reconstruction is shown in Fig. 4(d), with misleading voids and enhanced edges as a result of the non-monotonic projection images, as reported elsewhere.^{10,11} The signals were then binarized to extract the shadows (i.e., pixels with nonzero values). The shape-from-silhouette (SFS) technique¹² was applied to the shadow-transformed tilt series to estimate the outer shape of the cross section [Fig. 4(f)]. The SFS technique gives a reliable shape estimation for convex objects (as in our case here), subject to the same restrictions about the missing wedge. The estimated outer shape was then used as a mask in Fig. 4(e) to remove the star artefacts and extract the object from the background, as shown in Fig. 4(g).

In summary, EDX tomography is a promising technique for the reconstruction of specimens on the nanoscale, tolerating larger maximum object thickness than any other standard TEM/STEM imaging mode. It will be instructive in the future to compare our method for $>1 \mu\text{m}$ sized objects with the large-angle BF-STEM technique proposed by Ercius *et al.*,¹⁰ who predict based on simulations a similar high thickness range of applicability. The major advantage of EDX

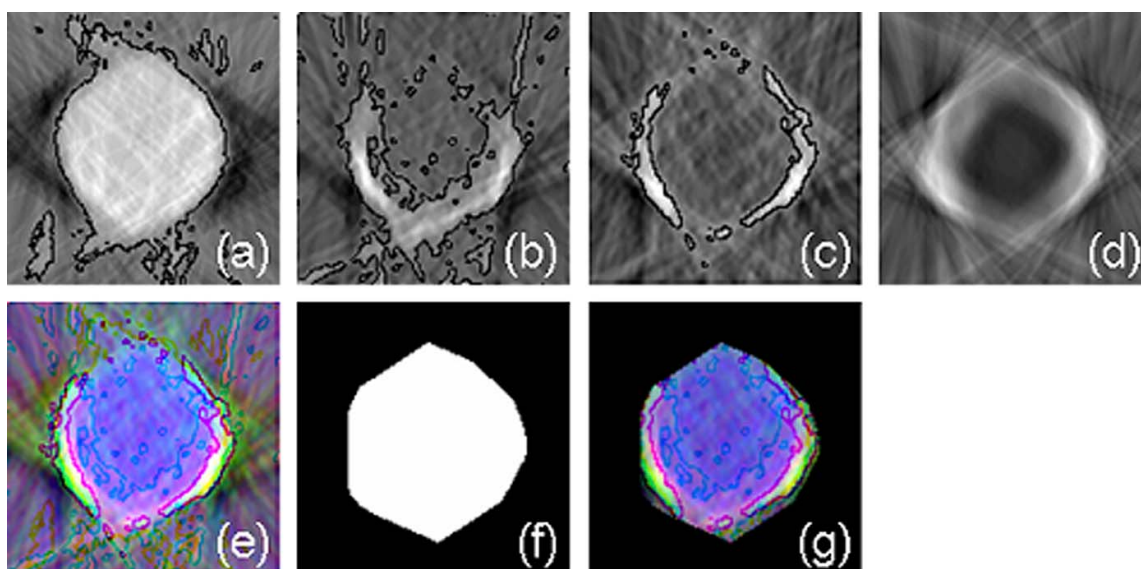


FIG. 4. (Color online) EDX tomographic reconstruction of the chemical distribution of (a) $W L\alpha$, (b) O-K, and (c) C-K in the cross section along AB. Line contours were added to emphasize the compositional variations. (d) ADF-STEM reconstruction of the cross section with enhanced edges and artificial voids. The RGB map in (e) shows the superposition of $W L\alpha$ and O-K in the shell and in the carbon contamination layer. (f) The convex hull of the cross section was estimated from ADF-STEM "shadows" and (g) used as a mask to reduce the backprojection artefacts (g).

tomography is the spectroscopic sensitivity allowing 3D chemical mapping, while the long acquisition time imposes a large tilt increment which limits the resolution of the reconstruction. However, if combined with ADF-STEM geometric tomography by multiplication of two tomograms, a crisp surface and a subsurface chemical information can be obtained simultaneously.

This work was supported by a grant from EPSRC (GR/S85689/01) UK.

¹T. Kuzumaki, S. Kitakata, K. Enomoto, T. Yasuhara, N. Ohtake, and Y. Mitsuda, *Carbon* **42**, 2343 (2004).

²T. Motoki, W. Gao, S. Kiyono, and T. Ono, *Meas. Sci. Technol.* **17**, 495 (2006).

³Y. Zhu, C. Ke, and H. D. Espinosa, *Exp. Mech.* **47**, 7 (2007).

⁴M. S. Bobji, J. B. Pethica, and B. J. Inkson, *J. Mater. Res.* **20**, 2726 (2005).

⁵J. Frank, *Electron Tomography: Methods for Three-dimensional visualization of Structures in the Cell* (Plenum, New York, 2007).

⁶G. Möbus and B. J. Inkson, *Appl. Phys. Lett.* **79**, 1369 (2001).

⁷P. A. Midgley and M. Weyland, *Ultramicroscopy* **96**, 413 (2003).

⁸G. Möbus, R. C. Doole, and B. J. Inkson, *Ultramicroscopy* **96**, 433 (2003).

⁹J. R. Kremer, D. N. Mastrorade, and J. R. McIntosh, *J. Struct. Biol.* **116**, 71 (1996).

¹⁰P. Ercius, M. Weyland, D. A. Muller, and L. M. Gignac, *Appl. Phys. Lett.* **88**, 243116 (2006).

¹¹Z. Saghi, X. Xu, and G. Möbus, "Electron Tomography of Regularly Shaped Nanostructures under Non-linear Image Acquisition," (submitted).

¹²A. Laurentini, *IEEE Trans. Pattern Anal. Mach. Intell.* **16**, 150 (1994).